Int. J. of Thermodynamics
Vol. 9 (No. 4), pp. 1-14, December 2006
ISSN 1301-9724

The Use of the 2nd Law as a Potential Design Tool for Aircraft Air Frame Subsystems

Kehinde Alabi*, Foluso Ladeinde.
Thaerocomp Technical Corp., P. O. Box 1527, Stony Brook, NY, 11790-0609

Michael von Spakovsky
Department of Mechanical Engineering, Virginia Tech, Blacksburg, VA, 24061-0238

and

David Moorhouse, Jose Camberos
Air Force Research Laboratory, Wright-Patterson Air Force Base, OH 45433-7542

Abstract

This paper presents the modeling of the irreversible thermodynamics of the Air Frame Subsystem as a component of integrated aircraft design/synthesis. Entropy calculation procedures for complicated geometries in curvilinear coordinates are described, including the effects of turbulence. Both inviscid and viscous calculations are reported and the contributions of the various terms in the entropy equation are investigated. The procedure is validated and then extended to the calculation of entropy generation associated with flow over the B747-200 aircraft. Results show that most of the entropy generation is due to turbulence. The viscous dissipation term in the entropy equation dominates compared to the heat transfer term. The implications of the results for design improvement are briefly discussed.

Keywords: Irreversible thermodynamics, 2nd law, airframe subsystem, entropy generation, turbulence modeling, viscous dissipation, irreversible heat transfer

1. Introduction

The design and optimization of a complete aircraft is a complicated undertaking consisting of many variables and requiring the convergence of technologies and experts from different disciplines. Engineers have tackled this problem by using decomposition procedures (Rancruel, 2002, Rancruel and von Spakovsky, 2004 and Munoz and von Spakovsky, 2003). In this approach, the complicated system consisting of many variables is broken up into subsystems, each possessing a certain degree of autonomy but depending on other subsystems via a smaller number of shared variables. The potential role of irreversible thermodynamic modeling as a single currency for the analysis/synthesis of each subsystem is of interest in the present work. An advantage of this approach lies in the fact that irreversible thermodynamic expressions can be compiled for virtually any subsystem type including those based on energy and non-energy metrics including aerodynamics and structural considerations.

A physical decomposition of a complete aircraft system may result in several subsystems, including the Air Frame-Aerodynamics, Air Frame-Structural, Propulsion, Environmental Control, Fuel Loop, Vapor Compression / PAO (polyalphaolefin) Loops Subsystem, Electrical, Hydraulic, Expendable Payload, Equipment Group, Permanent Payload, and Controls. The present paper focuses on the Air Frame Subsystem – Aerodynamics (AFS-A). Procedures for the irreversible thermodynamic modeling of this subsystem are presented. In particular, the contribution of the AFS-A subsystem to the overall entropy generation in a complete aircraft design/synthesis task is investigated.

Exergy and entropy-based methods are gaining increased use in system synthesis and design. This work extends the proposal by Moorhouse (2003) that a flight vehicle can be considered as a device to do work. Then every component is modeled in terms of exergy destruction, i.e., entropy generation, and can be optimized to a system-level metric. Compared to energy-based formulations which deal with the conversion and conservation of energy, entropy-based analysis provides additional information on the quality of energy or the energy that is

*Author to whom correspondence should be addressed

available for useful work. Adeyinka and Naterer (2002) presented irreversible thermodynamic calculations of loss analysis based on entropy generation rate that is consistent with traditional energy-based loss correlations and used the procedure to select optimal diffuser geometry for the least losses. Natalini and Sciubba (1995) used local entropy generation results to suggest areas for improvement in turbomachinery designs. Adeyinka and Naterer (2004) showed that the flow losses in pipes could be directly measured by the entropy generation rate. A detailed review of entropy and its significance in irreversible thermodynamic modeling is presented by Naterer and Camberos (2003).

In spite of the potential advantages of 2nd law based modeling for the CFD modeling of engineering systems, entropy-based simulations provide a challenge because of the scarcity of experimental data to validate computations (Adeyinka and Naterer 2004). As a result, many entropy-based studies have relied on analytic solutions for validation, using simple canonical problems. To our knowledge, entropy-based procedures have not yet been applied to entire aircraft geometry. One objective of the current work is to demonstrate the viability of entropy-based methods for realistic engineering and geometrically complicated fluid dynamic problems. In addition, a representation of losses in terms of entropy generation offers significant insight into the flow and thermal transport phenomena over the air frame and provides an effective tool for improving performance. For the AFS-A, the general areas for design improvement could include the shape of the fuselage, wing, the construction details of the leading and trailing edges, and the various appendages. After the flow and thermal fields have been computed, the local values of the thermal and mechanical entropy-generation rates can be obtained from the computation of the flow fields. The information may be used by the designer to detect, by inspection, the key areas that require a modification in order to obtain an optimized design. The integration of the irreversible thermodynamic data for AFS-A into the overall design/synthesis of a complete aircraft is the motivation for the present work. The next section presents the irreversible thermodynamic model used in the current paper and discusses issues related to the accuracy of the procedure. The third section presents results for the procedure applied to the Boeing 747-200 aircraft. Entropy generation from both inviscid and viscous calculations is reported. The details of the flow field are also analyzed pointing out potential for using the information to identify areas for possible design improvement.

2. The Irreversible Thermodynamic Procedure for Entropy Generation

For the engineering systems of interest in the present paper, the flows are turbulent which, combined with the complex geometries involved, tests the ability of any CFD tool to generate accurate design data. At a first glance, it would seem that accurate entropy generation data could be obtained by solving the evolution equation for the entropy per unit volume:

$$\frac{\partial \rho s}{\partial t}+\frac{\partial}{\partial x_j}\left(\rho u_i s+\frac{q_j}{T}\right)\equiv \dot{S}_{gen}\geq 0 \qquad (1)$$

As demonstrated in Bejan (1982), the right hand side of Equation (1) can be formulated as

$$\dot{S}_{gen}=\frac{k}{T^2}\left(\frac{\partial T}{\partial x_i}\right)^2+\frac{\tau_{ij}}{T}\left(\frac{\partial u_i}{\partial x_j}\right)$$

Assuming averaging in the manner of Reynolds averaged Navier-Stokes (RANS) modeling for a moment: $u_i=\bar{u}_i+u_i'$, where $\bar{u}_i$ is the average velocity and u_i' is the fluctuating velocity, we end up with the following equation for averaged entropy (Kramer-Bevan, 1992):

$$\begin{aligned}
&\bar{\rho}\frac{\partial \bar{s}}{\partial t}+\frac{\partial}{\partial x_i}\begin{pmatrix}\overline{\rho s u_i}+\bar{\rho}\overline{s'u_i'}+\bar{s}\overline{\rho' u_i'}+\bar{u}_i\overline{\rho' s'}+\overline{\rho' s' u_i'}\\ -k\overline{\ln\left[\bar{T}\left(1+\frac{T'}{\bar{T}}\right)\right]}\end{pmatrix}\\
&=k\frac{\partial}{\partial x_i}\ln\bar{T}\frac{\partial}{\partial x_i}\ln\bar{T}+k\overline{\frac{\partial}{\partial x_i}(\ln T)'\frac{\partial}{\partial x_i}(\ln T)'}\\
&\quad+\mu\left(\overline{\left(\frac{1}{T}\right)}\frac{\partial\bar{u}_i}{\partial x_j}\frac{\partial\bar{u}_i}{\partial x_j}+\overline{\left(\frac{1}{T}\right)}\overline{\frac{\partial u_i'}{\partial x_j}\frac{\partial u_i'}{\partial x_j}}\right.\\
&\quad+2\frac{\partial\bar{u}_i}{\partial x_j}\overline{\left(\frac{1}{T}\right)'\frac{\partial u_i'}{\partial x_j}}+\overline{\left(\frac{1}{T}\right)'\frac{\partial u_i'}{\partial x_j}\frac{\partial u_i'}{\partial x_j}}\\
&\quad+\overline{\left(\frac{1}{T}\right)}\frac{\partial\bar{u}_i}{\partial x_j}\frac{\partial\bar{u}_j}{\partial x_i}+\overline{\left(\frac{1}{T}\right)}\overline{\frac{\partial u_i'}{\partial x_j}\frac{\partial u_j'}{\partial x_i}}\\
&\quad+\frac{\partial\bar{u}_i}{\partial x_j}\overline{\left(\frac{1}{T}\right)'\frac{\partial u_j'}{\partial x_i}}+\frac{\partial\bar{u}_j}{\partial x_i}\overline{\left(\frac{1}{T}\right)'\frac{\partial u_i'}{\partial x_j}}\\
&\quad+\overline{\left(\frac{1}{T}\right)'\frac{\partial u_i'}{\partial x_j}\frac{\partial u_j'}{\partial x_i}}\\
&\quad-\frac{2}{3}\left(\overline{\left(\frac{1}{T}\right)}\frac{\partial\bar{u}_i}{\partial x_i}\frac{\partial\bar{u}_k}{\partial x_k}+\overline{\left(\frac{1}{T}\right)}\overline{\frac{\partial u_i'}{\partial x_i}\frac{\partial u_k'}{\partial x_k}}\right.\\
&\quad\left.\left.+2\frac{\partial\bar{u}_i}{\partial x_i}\overline{\left(\frac{1}{T}\right)'\frac{\partial u_k'}{\partial x_k}}+\overline{\left(\frac{1}{T}\right)'\frac{\partial u_i'}{\partial x_i}\frac{\partial u_k'}{\partial x_k}}\right)\right).
\end{aligned}$$

The terms $\left(\frac{1}{T}\right)'$ and $\overline{\left(\frac{1}{T}\right)}$ need to be modeled in the foregoing equations, with the understanding that $\frac{1}{\overline{T}} \neq \overline{\left(\frac{1}{T}\right)}$.

Entropy generation obtained from the solution of the entropy transport equation will probably not be accurate due to cumulative numerical errors in the iterative process and the difficulty associated with closing the turbulence terms. Formulations based on the Onsager relations (Bejan, 1982) are preferred as they do not require iteration and have turbulent terms that are easier to close. This relation is quasi-steady:

$$\dot{S}_{gen} = \frac{1}{T}\tau_{ij}\frac{\partial u_i}{\partial x_j} - \frac{q_k}{T^2}\frac{\partial T}{\partial x_k} \qquad (2)$$

where the term on the left-hand side represents the entropy generation per unit volume. The first term on the right had side represents irreversibilities associated with the degradation of mechanical energy into internal energy (Natalini and Sciubba, 1995) while the second term represents irreversibilities associate with heat transfer across finite temperature differences.

Although Equation (2) appears to be more convenient for calculating entropy generation compared to the transport equation, it has some of the turbulence modeling problems associated with the viscous dissipation and heat flux-temperature gradient correlation, which can be written as $\overline{\frac{1}{T}\tau_{ij}\frac{\partial u_i}{\partial x_j}}$ and $\overline{\frac{-q_i}{T^2}\frac{\partial T}{\partial x_i}}$, respectively. Note that these terms can be expanded as follows:

$$\overline{\frac{1}{T}\tau_{ij}\frac{\partial u_i}{\partial x_j}} = \mu\overline{\left(\begin{array}{l}\frac{1}{2}\left(\frac{1}{T}\frac{\partial u_i^2}{\partial x_j} + 2\frac{1}{T}\frac{\partial u_j}{\partial x_i}\frac{\partial u_i}{\partial x_j} + \frac{1}{T}\frac{\partial u_j^2}{\partial x_i}\right) \\ -\frac{2}{3}\frac{1}{T}\frac{\partial u_i}{\partial x_i}\frac{\partial u_k}{\partial x_k}\end{array}\right)}$$

$$= \mu\left[\overline{\left(\frac{1}{T}\right)}\frac{\partial \overline{u}_i}{\partial x_j}\frac{\partial \overline{u}_i}{\partial x_j} + \overline{\left(\frac{1}{T}\right)}\overline{\frac{\partial u'_i}{\partial x_j}\frac{\partial u'_i}{\partial x_j}} + 2\frac{\partial \overline{u}_i}{\partial x_j}\overline{\left(\frac{1}{T}\right)'\frac{\partial u'_i}{\partial x_j}}\right.$$

$$+\overline{\left(\frac{1}{T}\right)'\frac{\partial u'_i}{\partial x_j}\frac{\partial u'_i}{\partial x_j}} + \overline{\left(\frac{1}{T}\right)}\frac{\partial \overline{u}_i}{\partial x_j}\frac{\partial \overline{u}_j}{\partial x_i} + \overline{\left(\frac{1}{T}\right)}\overline{\frac{\partial u'_i}{\partial x_j}\frac{\partial u'_j}{\partial x_i}}$$

$$+\frac{\partial \overline{u}_i}{\partial x_j}\overline{\left(\frac{1}{T}\right)'\frac{\partial u'_j}{\partial x_i}} + \frac{\partial \overline{u}_j}{\partial x_i}\overline{\left(\frac{1}{T}\right)'\frac{\partial u'_i}{\partial x_j}} + \overline{\left(\frac{1}{T}\right)'\frac{\partial u'_i}{\partial x_j}\frac{\partial u'_j}{\partial x_i}}$$

$$-\frac{2}{3}\left(\overline{\left(\frac{1}{T}\right)}\frac{\partial \overline{u}_i}{\partial x_i}\frac{\partial \overline{u}_k}{\partial x_k} + \overline{\left(\frac{1}{T}\right)}\overline{\frac{\partial u'_i}{\partial x_i}\frac{\partial u'_k}{\partial x_k}} + \right.$$

$$\left.\left. 2\frac{\partial \overline{u}_i}{\partial x_i}\overline{\left(\frac{1}{T}\right)'\frac{\partial u'_k}{\partial x_k}} + \overline{\left(\frac{1}{T}\right)'\frac{\partial u'_i}{\partial x_i}\frac{\partial u'_k}{\partial x_k}}\right)\right],$$

and

$$\overline{\frac{-q_i}{T^2}\frac{\partial T}{\partial x_i}} = k\overline{\frac{\partial}{\partial x_i}\ln T\frac{\partial}{\partial x_i}\ln T}$$

$$= k\frac{\partial}{\partial x_i}\overline{\ln T}\frac{\partial}{\partial x_i}\overline{\ln T} + k\overline{\frac{\partial}{\partial x_i}(\ln T)'\frac{\partial}{\partial x_i}(\ln T)'}\,.$$

We see that the terms on the right-hand side need to be modeled. This issue is a subject of ongoing research (Adeyinka and Naterer, 2004). The invocation of the so-called "Small Thermal Turbulence Assumption" proposed by Kramer-Bevan (1992) allows some calculations to be done but the basic modeling issues remain.

For the present studies, we have used an eddy viscosity-type formulation* to calculate the average entropy generation per unit volume:

$$\overline{\dot{S}}_{gen} = \frac{1}{\overline{T}}\overline{\tau}_{ij}\frac{\partial \overline{u}_i}{\partial x_j} - \frac{\overline{q}_k}{\overline{T}^2}\frac{\partial \overline{T}}{\partial x_k}\,, \qquad (3)$$

where eddy viscosity-type assumptions are made:

$$\overline{\tau}_{ij} = (\mu + \mu_T)\left(\frac{\partial \overline{u}_i}{\partial x_j} + \frac{\partial \overline{u}_j}{\partial x_i} - \frac{2}{3}\frac{\partial \overline{u}_k}{\partial x_k}\delta_{ij}\right),$$

and

$$\overline{q}_k = -\left(\frac{\mu}{Pr} + \frac{\mu_T}{Pr_T}\right)\frac{\partial \overline{T}}{\partial x_k}\,.$$

The average entropy generation rate can be expressed in non-dimensional form as follows:

$$\overline{\dot{S}}_{gen} = \frac{1}{Re}\frac{\mu+\mu_T}{\overline{T}}\left\{2\left(\frac{\partial \overline{u}}{\partial x}\right)^2 + \right.$$

$$2\left(\frac{\partial \overline{v}}{\partial y}\right)^2 + 2\left(\frac{\partial \overline{w}}{\partial z}\right)^2 -$$

$$\frac{2}{3}\left(\frac{\partial \overline{u}}{\partial x} + \frac{\partial \overline{v}}{\partial y} + \frac{\partial \overline{w}}{\partial z}\right)^2 + \left(\frac{\partial \overline{u}}{\partial y} + \frac{\partial \overline{v}}{\partial x}\right)^2 +$$

$$\left.\left(\frac{\partial \overline{u}}{\partial z} + \frac{\partial \overline{w}}{\partial x}\right)^2 + \left(\frac{\partial \overline{w}}{\partial y} + \frac{\partial \overline{v}}{\partial z}\right)^2\right\} \qquad (4)$$

$$+\frac{1}{(\gamma-1)M_\infty^2 Re\,Pr}\frac{\mu/Pr + \mu_T/Pr_T}{\overline{T}^2}$$

$$\left\{\left(\frac{\partial \overline{T}}{\partial x}\right)^2 + \left(\frac{\partial \overline{T}}{\partial y}\right)^2 + \left(\frac{\partial \overline{T}}{\partial z}\right)^2\right\}.$$

A coordinate transformation was used for the curvilinear coordinate system, such that

* Note that an LES calculation would have been preferred here as it might provide more accurate turbulent quantities in the boundary and shear layers but is out of computational reach for the current application and for many engineering problems of interest.

$$\frac{\partial u_i}{\partial x_j} = \frac{\partial u_i}{\partial \xi}\xi_{x_j} + \frac{\partial u_i}{\partial \eta}\eta_{x_j} + \frac{\partial u_i}{\partial \varsigma}\varsigma_{x_j} \ ,$$

$$\frac{\partial T}{\partial x_j} = \frac{\partial T}{\partial \xi}\xi_{x_j} + \frac{\partial T}{\partial \eta}\eta_{x_j} + \frac{\partial T}{\partial \varsigma}\varsigma_{x_j} \ .$$

It should be noted that integration over the volume of the entropy per unit volume is required to obtain the total entropy generation in the domain. Also, the above formulation allows the rate of entropy generation to be computed as a derived (post-processed) quantity.

Observations have shown that the contributions to the entropy generation rate due to viscous dissipation in Equation (4) show very steep gradients close to a wall and numerical simulations are far more effective with wall functions for the production terms (Adeyinka and Naterer, 2004; Kock and Herwig, 2004; Thaerocomp, 2004). This is particularly important for simulations with large values of y^+ (necessary when it is computationally impractical to resolve the flow at the wall for large calculations). The high Reynolds number k–ε model employs wall functions in place of fine resolutions at the wall and has been used for turbulent entropy calculations (Thaerocomp, 2004). The details of the model are presented below.

2.1 Turbulence viscosity models

The turbulent shear stress is approximated in eddy viscosity form:

$$\tilde{\tau}'_{ij} = 2\tilde{\mu}_T\left[\tilde{S}_{ij} - \frac{1}{3}\frac{\partial \tilde{u}_k}{\partial x_k}\delta_{ij}\right] - \frac{2}{3}\tilde{\rho}k\delta_{ij} \ ,$$

where $k = \frac{1}{2}\left(u'^2 + v'^2 + w'^2\right)$ is the turbulent kinetic energy, $\tilde{S}_{ij} = \frac{1}{2}\left(\frac{\partial \tilde{u}_i}{\partial x_j} + \frac{\partial \tilde{u}_j}{\partial x_i}\right)$ is the mean strain rate, $\mu_t = C_\mu f_\mu \frac{\rho k^2}{\varepsilon}$ is the eddy viscosity, and ε is the dissipation rate of k. The following equations are solved for k and ε:

$$\frac{\partial k}{\partial t} + \tilde{u}_j\frac{\partial k}{\partial x_j} - \frac{1}{\rho}\frac{\partial}{\partial x_j}\left(\left(\tilde{\mu} + \frac{\tilde{\mu}_t}{\rho_k}\right)\frac{\partial k}{\partial x_j}\right) = P - \varepsilon$$

$$\frac{\partial \varepsilon}{\partial t} + \tilde{u}_j\frac{\partial \varepsilon}{\partial x_j} - \frac{1}{\rho}\frac{\partial}{\partial x_j}\left(\left(\tilde{\mu} + \frac{\tilde{\mu}_t}{\rho_\varepsilon}\right)\frac{\partial \varepsilon}{\partial x_j}\right) = \frac{C_1}{\rho}\frac{\varepsilon}{k}P - \frac{C_2\varepsilon^2}{k}$$

The constants in the equations are $C_\mu = 0.09$, $\rho_\kappa = 1.0$, $\rho_\varepsilon = 1.3$, $C_1 = 1.44$, $C_2 = 1.92$ and $P = \tilde{\tau}_{ij}\tilde{S}_{ij}$ is the turbulent production. For boundary conditions, a two layer "law of the wall" was used to impose the k and ε values at the first point (on the wall). A wall function was also used in the viscous sublayer (Steffen, 1993; Ladeinde et. al., 2006).

2.2 Numerical procedures

A high-order, finite-difference scheme in curvilinear coordinate system in used to solve the Navier-Stoke equation of the flow field. In standard notations, the filtered Navier-Stokes equations can be written as

$$\frac{\partial \hat{U}}{\partial t} + \frac{\partial}{\partial \xi_i}\left(\hat{F}_i - \frac{1}{Re}\hat{F}_{v_i}\right) = 0 \qquad (5)$$

where $\hat{F}_i, \hat{F}_{v_i}$ are the flux and viscous terms respectively in the coordinate directions, *i*.

For spatial differencing, the procedure utilizes high-order compact scheme for subsonic calculations and the WENO scheme for high speed flows. A second order Beam-Warming procedure is used for time integration. Details of the numerical procedure can be obtained in (Ladeinde et. al., 2006, Thaerocomp, 2004).

3. Results

The numerical procedures used in the current work have been validated using several applications including the Onera wing, Sajben duct, NACA0012, RAE2822 airfoils, backward-facing step, and Woodward and Colella's rarefaction fan (Cosmin et. al., 2006; Ladeinde et. al., 2006). Validations of the entropy generation calculation were additionally carried out using a laminar and turbulent channel flow, details of which are provided in this section.

3.1 Laminar flow through a channel

The procedures described above have been used to calculate the flow between two flat parallel plates, similar to the calculations of Erbay et. al. (2003). This flow has been studied analytically and computationally by several investigators (Kakac and Yener, 1995; Sahin, 2000; Mahmud and Fraser, 2002; Erbay et. al., 2003). The physical system is illustrated in *Figure 1*. The plates are separated by a distance H in the y-direction. The length of the channel, L, is $10H$ aligned parallel to the x-axis. The channel walls are set at a temperature, $T_w = 1.1T_\infty$.

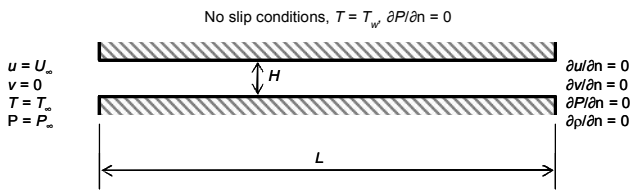

Figure 1. Boundary conditions for flow through a channel.

The flow equations are solved in a compressible form, therefore, the temperature

values are imposed by allowing the density to vary consistently with the computed pressures to satisfy the equation of state for a perfect gas. For instance, to set T_w, the density is imposed as follows:

$$\rho_w = \frac{\gamma Ma^2}{T_w} .$$

The computational grid used is 200 x 50 with high mesh gradients close to the wall and y^+ = 0.064. The Reynolds number Mach number and are 100 and 0.0, respectively. The compact scheme was used for spatial differencing while the Beam-Warming scheme was used for differencing in time. A fixed time step size of 0.0005, was imposed with four sub-iterations for convergence within each time step. An initial condition of $u = 0$ and $P = 1/\gamma Ma^2$ was imposed. The simulation was run until steady state at a non-dimensional time of approximately $T = 5$.

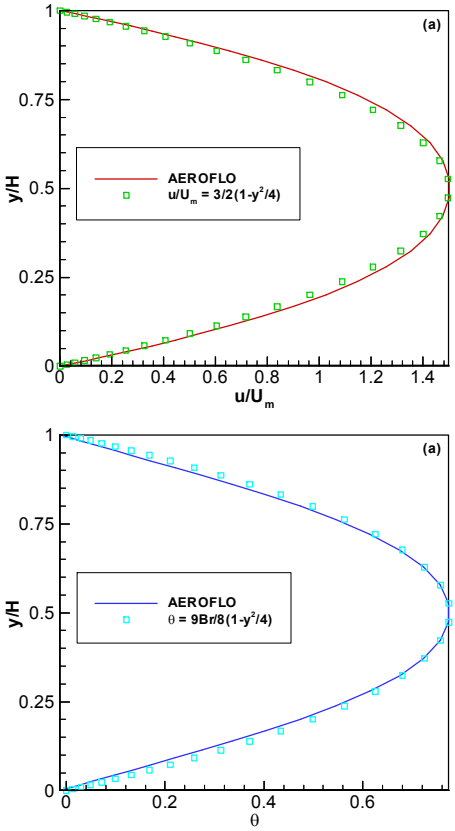

Figure 2. (a) u/U_m and (b) θ profiles compared with analytic solutions in the fully develop region.

Figure 2 shows comparison of the resulting flow field compared with analytic solutions in the fully developed region at x/H = 9 (Kakac and Yener, 1995). The results show good agreement.

The average Nusselt number, *Nu*, at the wall was computed as 7.14 compared with the analytic value of 7.534 (Kakac and Yener, 1995). *Nu* is defined by the following expression:

$$Nu = \frac{q''}{T_w - T_\infty} = \frac{-\left.\frac{\partial T}{\partial y}\right|_{y=wall}}{T_w - 1} .$$

Figure 3 shows the Nusselt number profile at the wall for the current calculations compared with the calculations of Erbay et. al. (2003). The results show good agreement except close to the inlet region. Note that in order to satisfy the equation of state, the density at the walls has an imposed value of 1/1.1.

Figure 4 shows the *u*-velocity, temperature and entropy contours, which show good agreement with the plots presented by Erbay et. al. (2003) (not shown).

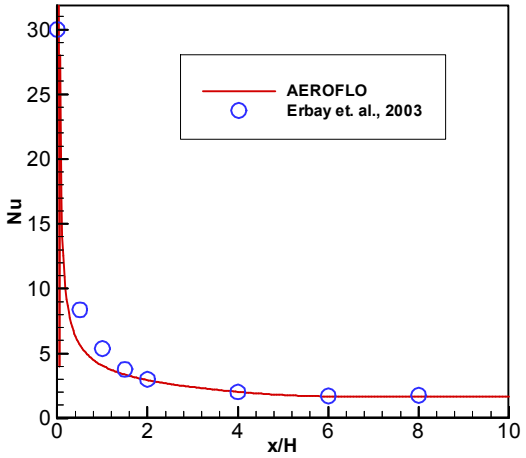

Figure 3. Nusselt number at the wall compared to solutions of Erbay et. al (2003).

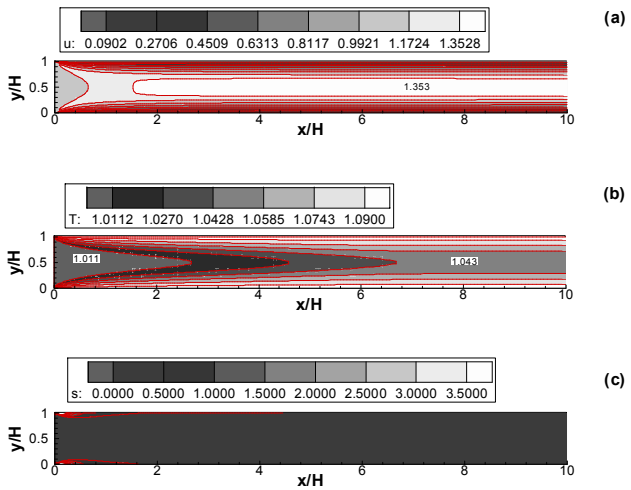

Figure 4. Contours of (a) u, (b) T, and (c) s for T_w/T_∞ = 1.1.

In order to determine the major contributions to entropy production, the following quantities from Equation (3): $\frac{1}{\bar{T}}$, $\frac{1}{\bar{T}^2}$, $\frac{1}{Re}\frac{1}{\bar{T}}\bar{\tau}_{ij}\frac{\partial \bar{u}_i}{\partial x_j}$, and

$$\frac{1}{(\gamma-1)M_\infty^2\,\mathrm{Re}\,\mathrm{Pr}}\frac{1}{\bar{T}^2}\left(\frac{\partial \bar{T}}{\partial x_j}\right)^2$$ were examined.

Figure 5 shows their relative values. The calculations show that over 90% of the entropy generation is due to viscous dissipation. This is consistent with the observations of Adeyinka and Naterer (2004). In general, most of the entropy is generated in the entry or inlet region or the developing region. This is mostly due to the large velocity and temperature gradients that develop from the inlet prior to establishing a smooth temperature and velocity transition from the wall values.

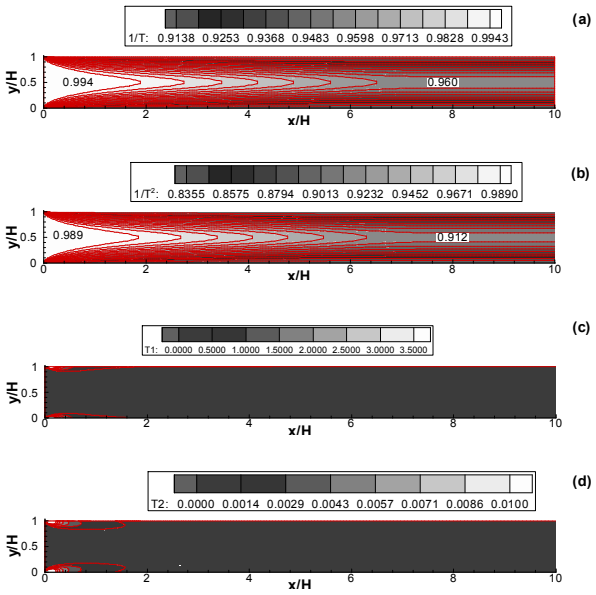

Figure 5. Contours of (a) $\frac{1}{\bar{T}}$, *(b)* $\frac{1}{\bar{T}^2}$, *(c)* $\frac{1}{\mathrm{Re}}\frac{1}{\bar{T}}\bar{\tau}_{ij}\frac{\partial \bar{u}_i}{\partial x_j}$, *and (d)* $\frac{1}{(\gamma-1)M_\infty^2\,\mathrm{Re}\,\mathrm{Pr}}\frac{1}{\bar{T}^2}\left(\frac{\partial \bar{T}}{\partial x_j}\right)^2$ *for* $T_w/T_\infty = 1.1$.

3.2 Turbulent flow through a channel

The turbulent channel flow calculation is based on the same geometry as that reported in 3.1, except that the grid used is 300 x 140 and the Reynolds number is in the range $7\times10^3 \le \mathrm{Re} \le 50\times10^3$. In addition, the high-Reynolds number k–ε turbulence model is used. This calculation is intended to validate the eddy viscosity model used for entropy calculations in the present paper. The entropy generation rate in the fully developed section of the channel is presented in *Figure 6*. (Adeyinka and Naterer, 2004) related the friction factor for a turbulent pipe flow to the entropy generation in the developed section using the following equation:

$$f = \frac{4}{\rho \bar{u}^3}\int \bar{T}\dot{\bar{S}}_{gen}\,dy \qquad (5)$$

Figure 6(b) shows the comparison of the current calculations using Equation (5) with the Colebrook equation with good agreement.

3.3 Calculation of flow over Boeing 747-200 commercial aircraft

The entropy production associated with the flow over a Boeing 747-200 commercial aircraft was calculated as a way of generating exergy-based design data for the AFS-A subsystem of an integrated aircraft design/synthesis analysis. The following conditions were used: $M_\infty = 0.855$,

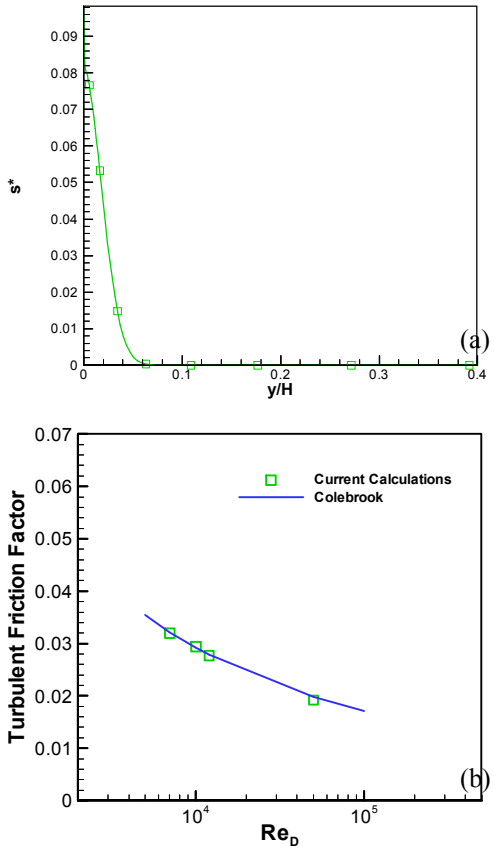

Figure 6. (a) Entropy distribution at Re = 10,000 and (b) friction factor compared with Colebrook equations for flow through a turbulent channel.

α = 3.05°, reference area = 511 m^2 (5500 sq ft), moment center = (34, 0, 4.8735) m, moment reference length, L_{ref} = 8.326 m, and Re/L_{ref} = 420368.7/m. The spatial dimensions have been normalized with the moment reference length, leading to a reference Reynolds number, $Re = 3.5\times10^6$. In the above, the moment center is chosen as the location where the aerodynamic moment remains roughly constant with the angle of attack and the moment reference length is chosen as the mid-span wing chord length. Both Euler and Navier-Stokes calculations were carried out using

high-order discretization. The computational grids contained nine blocks with the following grid points: fuselage 138 x 70 x 30 = 416,000, nose cone 31 x 20 x 30 = 18,600, tail cap $(31\times 20\times 30 = 18{,}600)$, wing base 129 x 38 x 30 = 147,060, wing mid section 50 x 129 x 29 = 187,050, wing tip (top) 77 x 41 x 28 = 81,508, wing tip (bottom) 77 x 41 x 28 = 81,508, wing patch 71 x 71 x 71 = 357,911, and far-field grid 73 x 39 x 48 = 136,656. This yields a total number of grid points of 1,444,993. The first grid at the wall is located approximately at Δy = 1 x 10^{-4} which corresponds to a $y^+ \approx 80$. The grid used for the calculations is shown in *Figure 7* and described below.

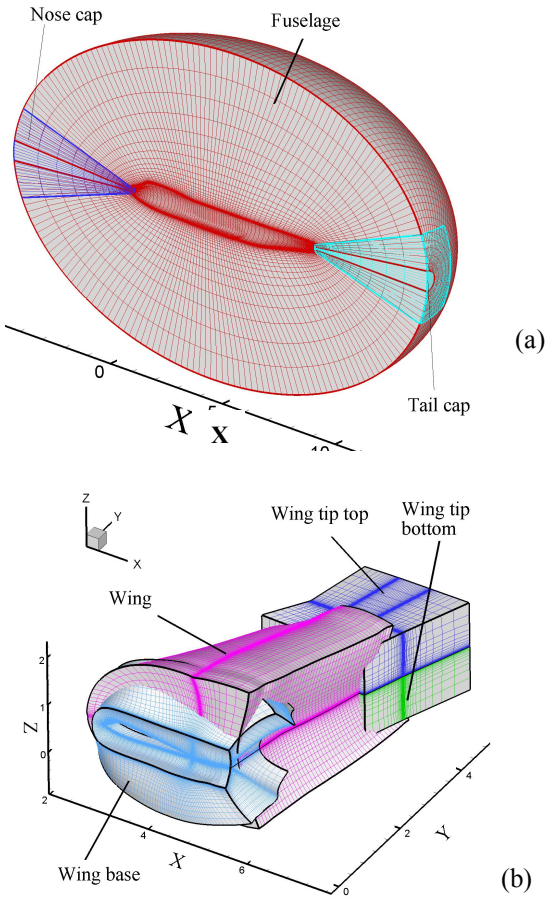

Figure 7. Mesh used for the computation of flow around the B747-200.

3.3.1 The B747-200 overset grid system

The fuselage surface is modeled using three overset blocks shown in *Figure 7(a)*. Block 2 (fuselage) spans most of the fuselage length in the physical *x*-direction. Blocks 3 and 4 are designed to cover the nose and tail surfaces of the fuselage. The later blocks are necessary to avert the computational singularities near the two poles.

Figure 7(b) shows an ensemble view of the computational grids, Blocks 5 through 8, around the wing. Block 5 (wing base) is a C-H type grid designed to connect the wing and fuselage surfaces. Block 6 (wing) is a C-type grid and extends over most of the wing span. Blocks 7 and 8 (wing tip top and bottom) consist of the H-H topology.[†] The computational blocks around the wing exhibit enhanced grid density near the wing trailing edge and near the wing tip. For all computational blocks near solid walls (Blocks 2 through 8) the normalized grid space value at the wall is $\Delta = 1\times 10^{-4}$.

A far-field box-shaped grid (not shown in *Figure 7*) is designed to connect the computational blocks near the fuselage and the wing with far field conditions. For Block 1, the grids are clustered near the fuselage and wing blocks in all computational directions.

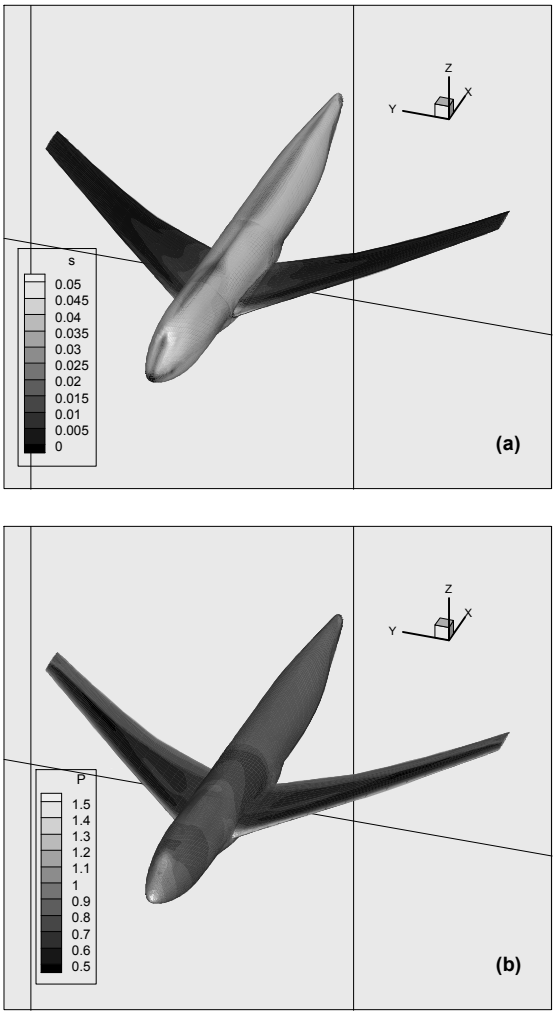

Figure 8. Contours of (a) entropy generation and (b) pressure around the B747-200 aircraft.

Details of the calculation and some of the difficulties encountered in performing the

[†] The C and H designation simply denote the geometric topology of the grid blocks where the C grid is one single grid curved with the ends of the grid approximately coinciding in the same direction and H grids are adjacent grids with two sides coinciding in the same direction like the letter H.

Figure 11 shows the eddy viscosity plots at the same sections as in *Figure 10*. The results show a correspondence between the areas of high eddy viscosity and entropy generation.

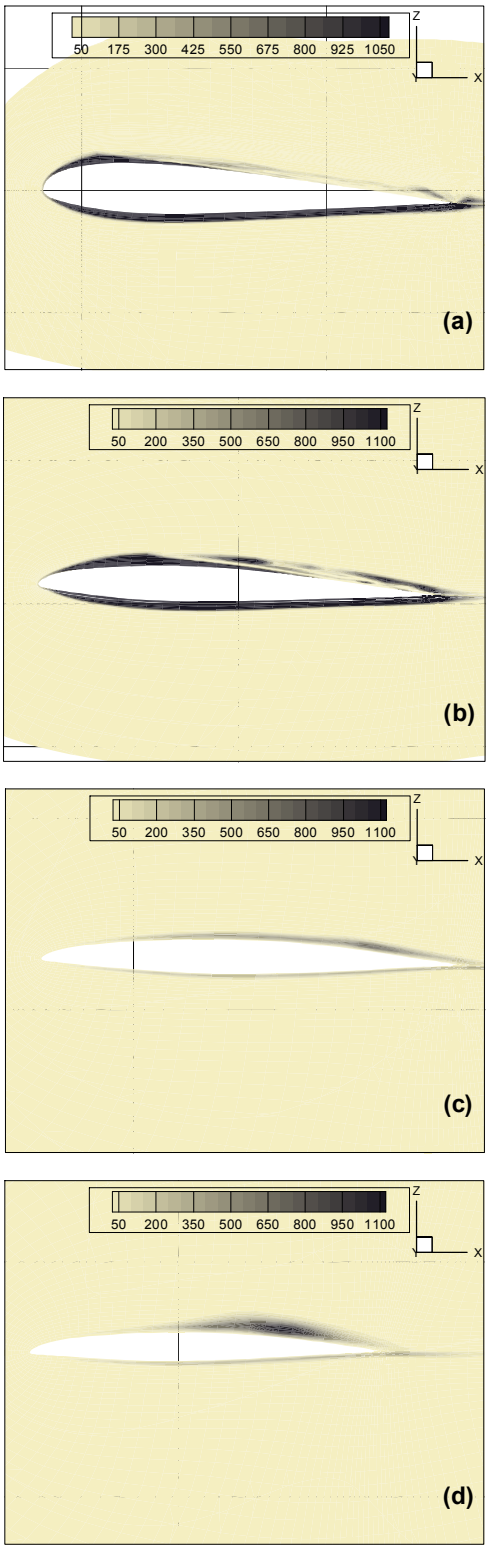

Figure 11. Eddy viscosities at various wing locations: (a) 14%, (b) 28%, (c) 42%, and (d) 71%.

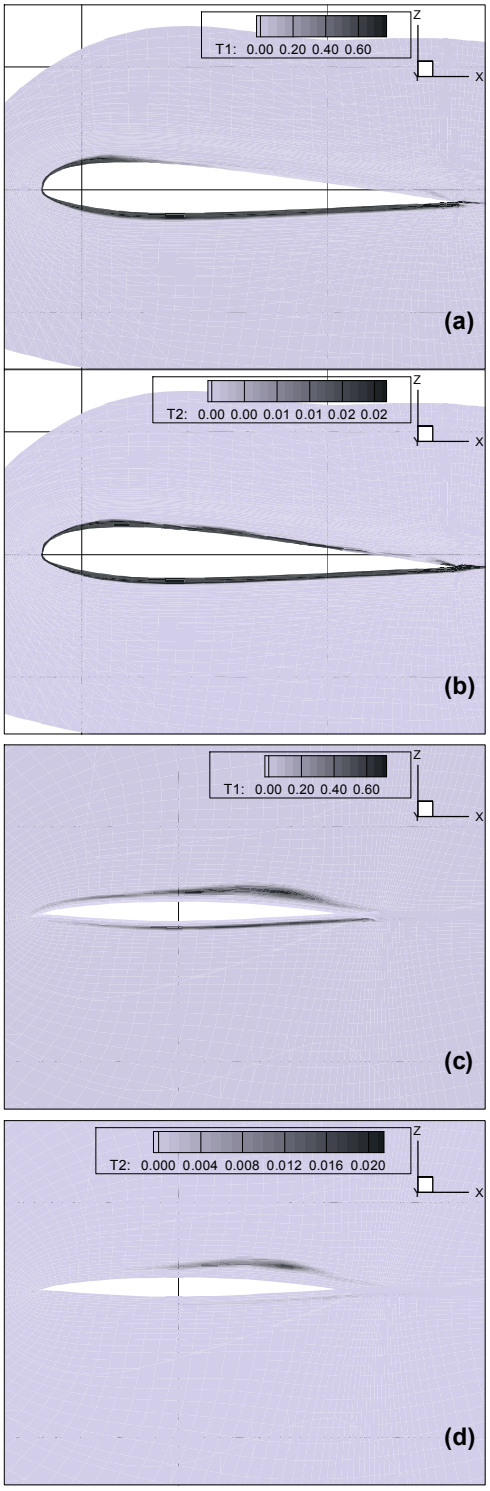

Figure 12. Entropy components $T1 \equiv \frac{1}{\mathrm{Re}} \frac{1}{\overline{T}} \overline{\tau}_{ij} \frac{\partial \overline{u}_i}{\partial x_j}$ *and* $T2 \equiv \frac{1}{(\gamma-1) M_\infty^2 \,\mathrm{Re}\,\mathrm{Pr}} \frac{1}{\overline{T}^2} \left(\frac{\partial \overline{T}}{\partial x_j} \right)^2$ *at 14% and 71% wing locations: (a) T1 at 14%, (a) T2 at 14%, (c) (a) T1 at 71%, and (d) T2 at 71%.*

Figure 12 shows the relative contributions of the viscous dissipation-related term,

$$T1 \equiv \frac{1}{Re}\frac{1}{\overline{T}}\overline{\tau}_{ij}\frac{\partial \overline{u}_i}{\partial x_j}, \text{ and}$$

$$T2 \equiv \frac{1}{(\gamma-1)M_\infty^2 \, Re \, Pr}\frac{1}{\overline{T}^2}\left(\frac{\partial \overline{T}}{\partial x_j}\right)^2, \text{ the heat transfer-related term (Equation 3) to the entropy generation rate at 14% and 71% wing locations. The figures show that most of the entropy generation is due to viscous dissipation. However, closer to the fuselage (at the wing-fuselage junction), the heat transfer related term accounts locally}^{\ddagger} \text{ for about 30% of the entropy generated and reduces to less than 5% further away from the fuselage. In the wing section from the base to about midpoint, the figure shows a high entropy generation close to the wing surface which reduces with the distance from the wing base. However, in the section between the midpoint and the wing tip, entropy generation increases on the suction side of the wing. In this section, there is provision for design improvement that will reduce the entropy generation rate on the suction side. In fact, as shown in *Figure 13*, the}$$

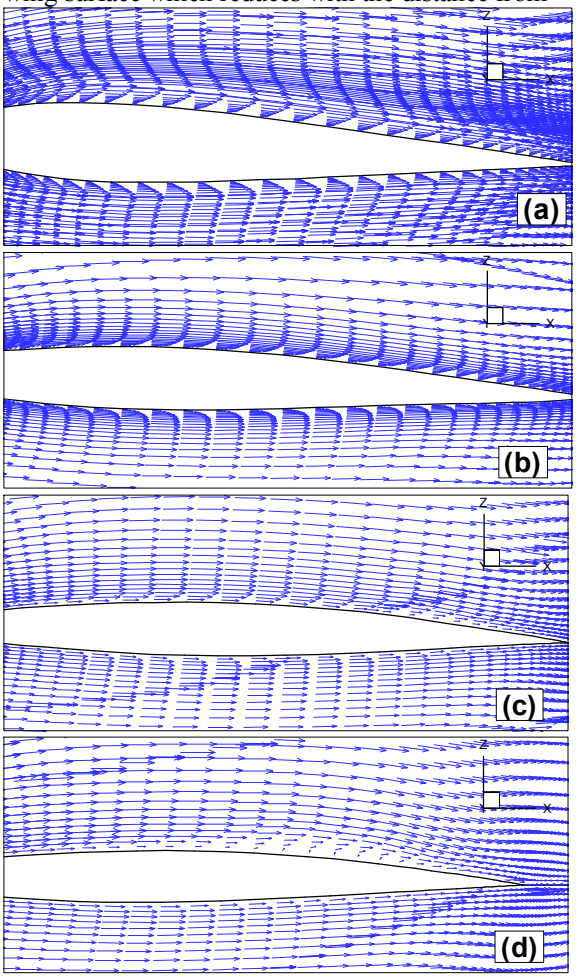

Figure 13. Velocity vectors at wing locations: (a) 14%, (b) 28%, (c) 42%, and (d) 71%.

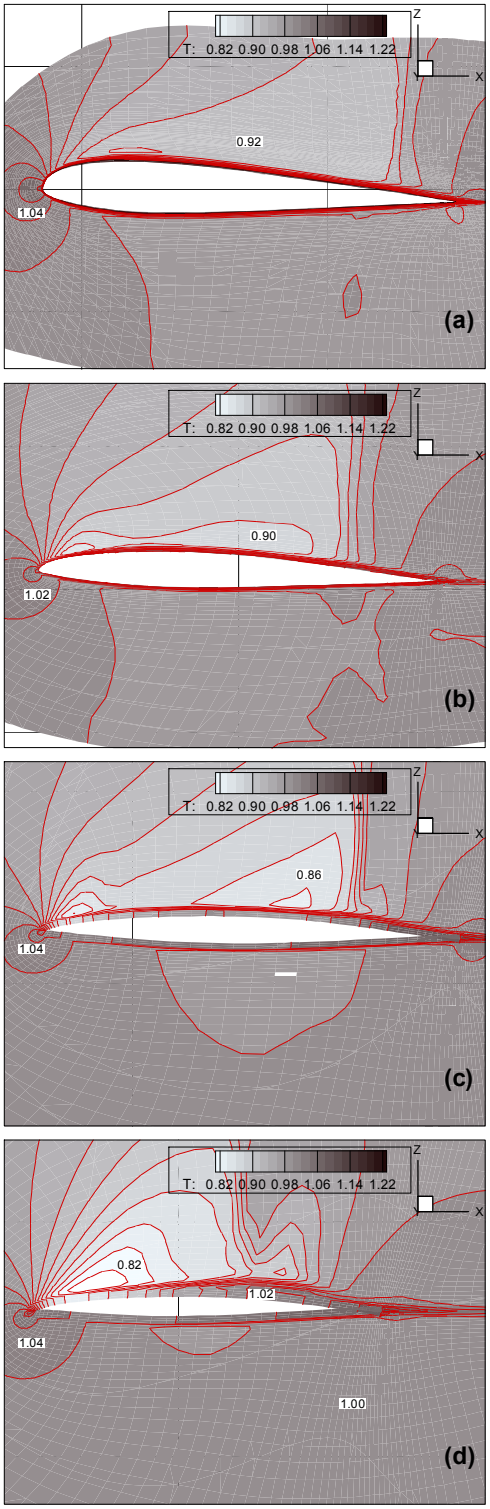

Figure 14. Temperature contours at wing locations: (a) 14%, (b) 28%, (c) 42%, and (d) 71%.

[‡] Note that the local region shown in Figure 11 in which the contributions of the heat transfer related entropy term is relatively enhanced coincides with the "temperature shock" region in Figure 14 and is slightly elevated above the boundary layer where the gradients of velocities are relatively smoother.

high entropy generation on the suction side of the wing observable at 71% wing location also coincides with the separation region.

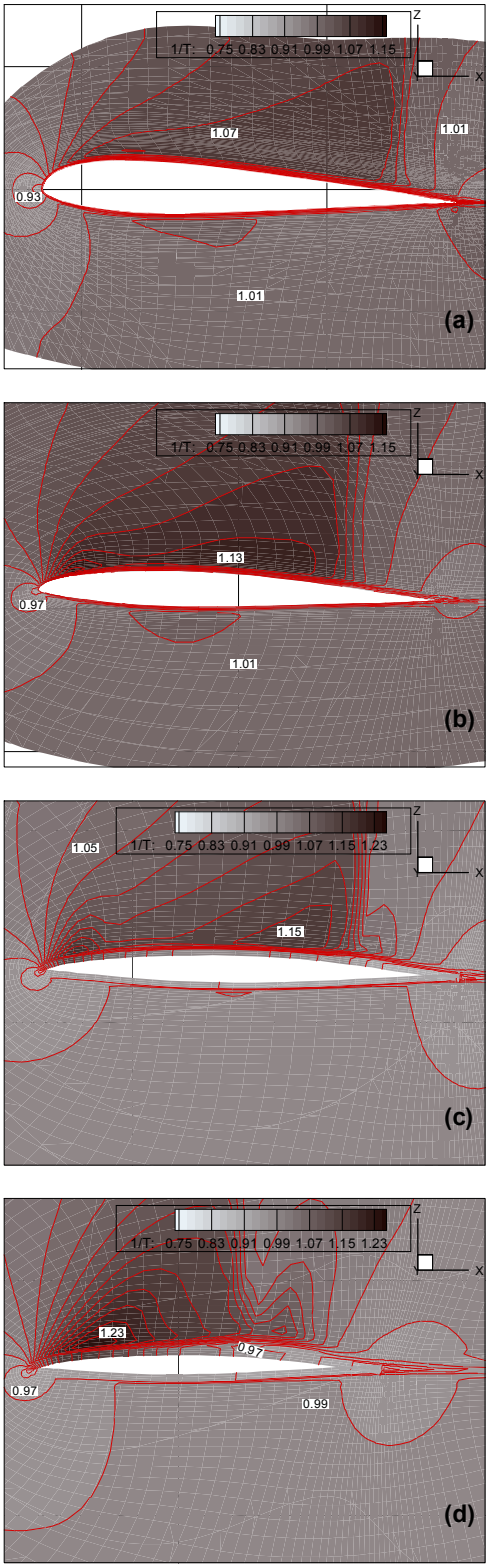

Figure 15 $1/\overline{T}$ *contours at wing locations: (a) 14%, (b) 28%, (c) 42%, and (d) 71%.*

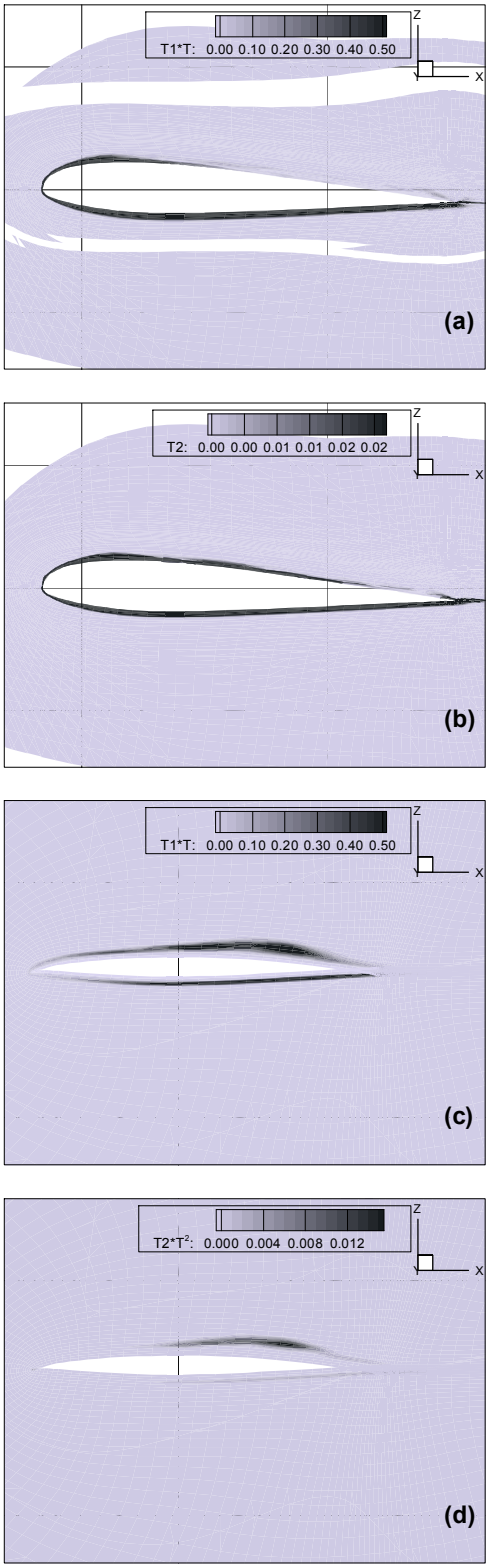

Figure 16. Entropy components

$$T1*\overline{T} \equiv \frac{1}{\mathrm{Re}}\overline{\tau}_{ij}\frac{\partial \overline{u}_i}{\partial x_j} \text{ and}$$

$$T2*\overline{T}^2 \equiv \frac{1}{(\gamma-1)M_\infty^2\,\mathrm{Re}\,\mathrm{Pr}}\left(\frac{\partial \overline{T}}{\partial x_j}\right)^2 \text{ at 14\% and 71\%}$$

*wing locations (a) T1*T at 14%, (a) T2*T² at 14%, (c) (a) T1*T at 71%, and (d) T2* T² at 71%.*

Figure 14 shows the temperature around the fuselage at 14% and 71% wing locations. A weak shock in the temperature profile that coincides with the locations of high entropy generation can be observed. This region has high temperature gradients and occurs around the slight separation bubble on the suction side of the wing. *Figure 15* shows the plot of $1/\overline{T}$ while *Figure 16* shows the plots of $\frac{1}{Re}\frac{1}{\overline{T}}\overline{\tau}_{ij}\frac{\partial \overline{u}_i}{\partial x_j}$, and $\frac{1}{(\gamma-1)M_\infty^2 Re Pr}\frac{1}{\overline{T}^2}\left(\frac{\partial \overline{T}}{\partial x_j}\right)^2$. These figures show that the gradient-related terms have larger contributions to entropy generation rate compared to $1/\overline{T}$ and $1/\overline{T}^2$.

3.3.3 Inviscid entropy generation

The total entropy generations from the inviscid calculations are summarized in Table I. The values of entropy generation are almost negligible compared with the viscous calculations. In fact, the entropy generation from the viscous calculations is approximately 1000 times that of the inviscid calculations. Most of the entropy generated was located in the boundary layer. Considering the eddy viscosity plot in *Figure 11*, it appears that the quantity, $(\mu + \mu_t)$, which has a magnitude of $\mu_t \approx 1000\mu$ accounts for most of the differences in the entropy production between both models. As noted by Denton (1993), the entropy generated from the inviscid calculations is mostly due to numerical dissipation and accounts for the low values observed in Table I. Details and plots of the results of the inviscid calculations can be accessed in Alabi et. al. (2006).

TABLE I. TOTAL RATE OF ENTROPY GENERATION FOR EACH BLOCK.

Block	Inviscid	Viscous
Fuselage	2.06×10^{-6}	0.1044
Nose cap	8.70×10^{-8}	0.0014
Tail cap	2.66×10^{-7}	0.00042
Wing base	4.95×10^{-3}	0.02656
Wing	4.93×10^{-6}	0.02722
Wing tip top	8.53×10^{-7}	0.00313
Wing tip bottom	3.642×10^{-7}	0.0029
Wing patch	5.306×10^{-7}	1.4×10^{-4}
Far-field grid	$\sim 10^{-9}$	$\sim 10^{-9}$
Total Entropy	**4.96×10^{-3}**	**0.166**
Total Exergy (W)		**3.61×10^{8}**

The total exergy destruction or work potential lost can also be computed using the Guoy-Stodola relation, equating the rate of exergy destruction or irreversibilities occurring in a process to the rate of entropy generation via the "dead state" temperature, i.e.

$$\dot{I} = T_0 \dot{S}_{gen} = \dot{E}x$$

Taking the "dead state" temperature as environment temperature, the total rate of exergy destruction as well as the rate of entropy generation for each block are presented in TABLE I. Once again note that the entropy generation calculations for the inviscid case are primarily due to numerical generated dissipation.

4. Conclusion

The entropy generation around a B747-200 aircraft was analyzed using computational fluid dynamics. The contributions of the various terms in the entropy equation were assessed. Viscous and inviscid models were investigated. The calculations show that inviscid results are unable to provide accurate results for the entropy generation. In addition, it was determined that most of the entropy generation in the viscous calculations were due to the turbulent eddy viscosity which was about 1000 times the molecular viscosity in the application flow field. Comparison of the entropy generation terms associated with the viscous calculations shows that the viscous dissipation contributes approximately 90% of the total entropy production term, with the heat transfer-related term contributing the remaining 10%. In addition, the calculations show possibility of design improvement particularly in the wing sections removed away from the fuselage.

The results that have been presented may be considered as intuitively obvious and could give the design team what was expected. This is probably true for an evolutionary configuration like the B747-200. The authors suggest that their approach would be very productive as part of the integrated design of a configuration without pre-existing data. As an audit of a chosen configuration, this high-fidelity computation of entropy generation would identify the location and cause of "fuel waste". As the design team minimizes these effects, we would expect that there would be further benefits from other components in the total aircraft system that could be further optimized.

Acknowledgments

This work was funded by the United States Air Force under Contract FA8650-05-C-3521 via the Phase II SBIR program. The authors are very grateful to the Air Force for giving Thaerocomp the opportunity to develop innovative research tools.

Nomenclature

C_p pressure coefficient

f	friction factor
M_∞	free stream Mach number
J	Jacobian of the coordinate transformation matrix
k	turbulence kinetic energy
L_{ref}	reference length
Pr_T	turbulence Prandtl number
Re	Reynolds number ($\rho_\infty U_\infty L_{ref}/\mu_\infty$)
s	entropy generation
S_{ij}	"ij" component of the strain rate tensor
$\dot{S}_{gen}$	entropy generation rate per unit volume
T_w	wall temperature
γ	ratio of specific heats
t	time
u, v, w	velocity components in the x, y, z Cartesian coordinate directions, respectively
u_τ	friction velocity
U_∞	free stream velocity velocity
α	angle of attack
ρ_∞	free stream density
τ_{ij}	stress tensor
μ_∞	free stream viscosity

References

Adeyinka, O. B. and Naterer, G. F., 2004, "Modeling of Entropy Production in Turbulent Flows" *J. Fluid Eng.* Vol. 126, pp. 893-899.

Adeyinka, O. B. and Naterer, G. F., 2002, "Predicted Entropy and Measures with Particle Image Velocimetry" *AIAA* 2002-2090.

Alabi, K., Ladeinde, F., Safta, C., Cai, X., 2006, "Assessing CFD Modeling of Entropy Generation for the Air Frame Subsystem in an Integrated Aircraft Design/Synthesis Procedure", AIAA 2006-587. *44th Aerospace Sciences Meeting*, Reno, NV, January 2006.

Bejan, A., 1982, *Entropy Generation through heat and fluid flow*, J.Wiley & Sons, NY.

Denton, J. D., 1993, "Loss Mechanisms in Turbomachines" *J. Turbomach.* Vol. 115, Oct.

Erbay, L. B., Ercan, M. S., Sulus, B., and Yalcin, M. M., 2003, "Entropy Generation During Fluid Flow Between Two Parallel Plates with Moving Bottom Plate", *Entropy*, 5, 506-518.

Kakac, S. and Yener, Y., 1995, *Convective Heat Transfer*, CRC Press, 2nd ed.

Kock, F., Herwig, H., 2004, "Local Entropy Production in Turbulent Shear Flows: A High Reynolds Number Model with Wall functions", *Int. J. Heat Mass Transfer.*

Kramer-Bevan, J. S., 1992, "A Tool for Analysis of Fluid Flow Losses" *M.Sc Thesis*, University of Waterloo, Canada.

Ladeinde, F., Alabi, K., Safta, C., Cai, X., 2006, "The First High –Order Simulation of Aircraft: Challenges and Opportunities", AIAA 2006-1526. *44th Aerospace Sciences Meeting*, Reno, NV.

Mahmud,S., Fraser, R. A., 2002, "Thermodynamic Analysis of Flow and Heat Transfer Inside Channel with Two Parallel Plates", *Exergy, an International Journal*, vol. 2, pp. 140-146.

Moorhouse, D. J., 2003, "A Proposed System-Level Multidisciplinary Analysis Technique Based on Exergy Methods", *AIAA Journal of Aircraft*, Vol. 40, No. 1.

Muñoz, J.R., von Spakovsky, M.R., 2003, "Decomposition in Energy System Synthesis / Design Optimization for Stationary and Aerospace Applications", *AIAA Journal of Aircraft*, special issue, Vol. 39, No. 6.

Natalini G., Sciubba, E., 1995, "Minimization of the local rates of entropy production in the design of air-cooled gas turbine blades", *ASME J. Eng. for GT & Power*, v.121, pp 121-130.

Naterer, G. F., and Camberos, J. A., 2003, "Entropy Production Rates from Viscous Flow Calculations", *J. Thermophys. & Heat Transfer* 17(3), pp 360-371.

Rancruel, D. F., 2002, "A Decomposition Strategy Based on Thermoeconomic Isolation Applied to the Optimal Synthesis/Design and Operation of an Advanced Fighter Aircraft System", *M.Sc. Thesis*, Virginia State University.

Rancruel, D. F., von Spakovsky, M. R., 2004, "Use of a Unique Decomposition Strategy for the Optimal Synthesis/Design and Operation of an Advanced Fighter Aircraft System", 10th *AIAA/ISSMO* Multi- disciplinary Analysis and Optimization Conference, Aug. 30 - Sept. 1, Albany, New York.

Sahin, A. Z., 2000, "Entropy Generation in a Turbulent Liquid Fluid Flow Through a Smooth Duct Subjected to Constant Wall Temperature", *Int. Journal of Heat and Mass Transfer*, vol. 43, pp. 1469-1478.

Steffen, C. J.,1993, "A Critical Comparison of Several Low Reynolds Number k-ε Turbulence Models for Flow Over a Backward-Facing Step", *NASA Technical Memorandum* 106173. AIAA-93-1927.

Safta, C., Alabi, K., Ladeinde, F., 2006, "Comparative advantages of high-order schemes for subsonic, transonic, and supersonic flows", AIAA Paper AIAA-2006-299.

Thaerocomp Technical Corp., 2004, "*AEROFLO User's Manual*".